Biomedical Signal Processing and Control 103 (2025) 107428

Contents lists available at ScienceDirect

Biomedical Signal Processing and Control

journal homepage: www.elsevier.com/locate/bspc

Optimizing apnea–hypopnea event detection in pediatric OSAHS diagnosis: An enhanced genetic algorithm approach

Linwen Jiang, Min Li *, Jing Jiang, Qinghua Hu

School of Mechatronic Engineering and Automation, Shanghai University, Shanghai 200444, China

ARTICLE INFO

Keywords:
Pediatric OSAHS
Genetic algorithm
Apnea–hypopnea detection
Oxygen desaturation detection

ABSTRACT

Extensive evidence has demonstrated that analyzing oxygen desaturation patterns during night-time is a powerful tool in the diagnosis of obstructive sleep apnea–hypopnea syndrome (OSAHS). This paper presents an innovative genetic algorithm, referred to as ERD-GA, designed for diagnosing pediatric OSAHS. It incorporates an elitism retention strategy along with dynamic crossover and mutation probabilities, leading to a substantial improvement in diagnostic efficiency. Through a rigorous analysis of fluctuation patterns in blood oxygen saturation signals (SpO_2) and fine-tuning oxygen desaturation screening parameters, the algorithm demonstrates a high degree of proficiency in identifying obstructive apnea–hypopnea events. The validation has been performed on two separate datasets, comprising 36 and 318 pediatric subjects. Notably, it exhibited sensitivity rates of 97.83%, 91.67%, and 84.51% for classifying mild, moderate, and severe OSAHS cases, respectively. The results highlight the noteworthy advancements of the proposed algorithm in both oxygen desaturation detection and apnea–hypopnea detection. The intra-class correlation coefficient (ICC) values, measuring at 0.951 and 0.985 for the respective detections, indicate a high level of agreement with the PSG results. Additionally, the model demonstrates a substantial correlation with the gold standard PSG model in terms of the Apnea–Hypopnea Index (AHI). The Pearson's correlation coefficient values are 0.969 and 0.927 in the two datasets, respectively. These findings suggest that the proposed methodology signifies an innovative approach to diagnosing pediatric OSAHS and associated conditions.

1. Introduction

Obstructive sleep apnea–hypopnea syndrome (OSAHS) is an extremely common sleep-related breathing disorder (SRBD) that occurs during overnight sleep. OSAHS not only adversely impacts patients' sleep quality and daily functioning, but also induces hypertension, cardiovascular and cerebrovascular diseases and even death. Previous studies on OSAHS have predominantly focused on adult patients. However, due to the advancements in the field of sleep medicine, there is an increasing recognition of the prevalence of OSAHS in children.

Pediatric OSAHS is a common yet often underdiagnosed condition [1]. The primary risk factors for OSAHS are tonsillar hypertrophy and/or adenoid hypertrophy which can cause airway obstruction. This kind of disease is present in up to 5% of children [2]. The main clinical manifestations and complications associated with pediatric OSAHS include habitual snoring, abnormal breathing patterns, hidrosis, inattentiveness, daytime sleepiness, irritability and hyperactivity [3]. In young children, the symptoms of snoring are not so obvious. If unrecognized and untreated, OSAHS can lead to serious complications such as cor pulmonale in childhood [4,5] and increase the risk of hypertension and cardiovascular disease in their adulthood [6].

Polysomnography (PSG) is the gold standard for pediatric OSAHS diagnosis. The apnea–hypopnea index (AHI) is used to quantify the frequency of obstructive events per hour of sleep time [7]. According to the International Classification of Sleep Disorders, Third Edition (ICSD-3), pediatric OSAHS is defined as an AHI ≥ 1 [8]. The American Academy of Pediatrics (AAP) and American Academy of Sleep Medicine (AASM) recommend using nighttime PSG to diagnose sleep apnea before tonsillar hypertrophy surgery [9]. However, PSG is both costly and limited in availability. Furthermore, it requires specialized training to conduct PSG in children and assist their families in acclimating to the rigorous monitoring process. One particular challenge arises from the application of electrodes on the delicate skin of young children [10].

Overnight oximetry has emerged as a potentially useful screening approach due to its simplicity, portability, and suitability for children [11]. Brouillette et al. [12] reported that although oximetry had a positive predictive value of 97% and could be used to diagnose pediatric OSAHS, its sensitivity was only 43%. Catherine et al. [13]

* Corresponding author.
E-mail address: min_li@shu.edu.cn (M. Li).

https://doi.org/10.1016/j.bspc.2024.107428
Received 23 October 2023; Received in revised form 20 October 2024; Accepted 17 December 2024
Available online 30 December 2024

proposed that this method was best used in those with a high pre-test probability. Andy et al. [14] reported that the factor with the strongest correlation between AHI in infant PSG and pulse oximetry parameters was further analyzed using ROC for probable OSAHS screening.

Since a large number of pediatric apnea events are related to oxygen desaturation events, SpO_2 from oximetry has been proposed as a valuable tool for screening OSAHS in children. Moreover, OSAHS may cause intermittent hypoxemia at night. The duration of lowest oxygen saturation ($LSpO_2$) and the occurrence of SpO_2 dropping below 90% also represent the adverse effects of respiratory events during sleep time [15].

In recent years, promising results have been obtained in previous studies from the diagnosis of OSAHS based on SpO_2 variations. Various signal processing methods have been considered, including time-domain and frequency-domain techniques, as well as nonlinear methods [16–22]. Many methods were used to extract features (e.g., bispectrum [18], Empirical Mode Decomposition (EMD) [19], and Detrended Fluctuation Analysis (DFA) [21]). Then, machine-learning algorithms (e.g., Multilayer Perceptron (MLP) [18] and Multilayer Linear Regression (MLR) [21]) were combined with these methods to diagnose OSAHS. Most of these studies were based on features computed overnight to predict the occurrence of apnea events using trained oxygen features, without considering the time of onset and duration of each apnea–hypopnea event. Tang et al. [23] proposed a method for optimizing oxygen-desaturation-related parameters in OSAHS screening using a standard Genetic Algorithm (GA). However, the model's performance was constrained due to the limited number of experimental samples. Additionally, the standard GA approach posed challenges such as premature convergence and susceptibility to local optimal solutions.

In light of these considerations, this paper proposes an enhanced genetic algorithm referred to as ERD-GA. In this context, 'ERD' stands for 'Elitism Retention' in the elitism retention strategy and 'Dynamic' in dynamic crossover and mutation probabilities. The novelty of the ERD-GA lies in its superior classification performance in detecting both oxygen desaturation events and pseudo-oxygen desaturation events through the optimization of detection parameters. These findings establish a strong foundation for future studies, particularly in addressing the risk of underestimating the severity of OSAHS in pediatric patients experiencing prolonged individual oxygen desaturation events or hypopnea.

2. Materials and methods

2.1. Datasets

The first dataset used for this study comprises SpO_2 recordings from 36 children monitored simultaneously using PSG at Shanghai Children's Medical Center (SCMC). This dataset contains 3 children without OSAHS, 30 children with mild OSAHS, 1 with moderate, and 2 with severe OSAHS. The second dataset was obtained from the Children's Adenotonsillectomy Trial (CHAT) [24,25], a multicenter, single-blinded, randomized controlled clinical trial conducted at 6 academic sleep centers in the U.S. to assess neurophysiological and health outcomes in children with habitual snoring. From this pool, we selected the followup group (clinical trial identifier: NCT00560859) of 407 children who were randomly assigned to the treatment group. Approval to use CHAT was obtained at https://www.sleepdata.org/datasets/chat. With the exception of a small number of unreadable data files, 296 records were selected from the followup group of pediatric patients aged 5 to 9. Additionally, 22 baseline group records were selected to augment the sample size of severe pediatric OSAHS cases. Table 1 presents the demographic and clinical data of the subjects.

According to the AASM, AHI is used to quantify the frequency of apnea and hypopnea events per hour of sleep, and thus assess the severity of OSAHS. The assessment criteria are the same as those for OSAHS in the PSG report, as shown in Eq. (1).

Table 1
Demographic and clinical data of children under study.

	All	SCMC	CHAT
SpO_2 recordings (n)	354	36	318
Ages (years)	[3–13]	[3–13]	[5–9]
AHI (events/h)	3.15[0–29.45]	2.77[0.5–20.3]	3.19[0–29.45]
AHI < 1 (n)	137	3	134
1 ≤ AHI < 5 (n)	166	30	136
5 ≤ AHI < 10 (n)	20	1	19
AHI ≥ 10 (n)	31	2	29

Table 2
AHI-based criteria for diagnosing and grading OSAHS severity.

AHI (events/h)	Severity of adult OSAHS	AHI (events/h)	Severity of pediatric OSAHS
<5	None	<1	None
[5,15)	Mild	[1,5)	Mild
[15,30)	Moderate	[5,10)	Moderate
≥30	Severe	≥10	Severe

$$\begin{cases} AI = \frac{N_{apnea}}{T_{sleep}} \\ HI = \frac{N_{hypopnea}}{T_{sleep}} \\ AHI = AI + HI \end{cases} \tag{1}$$

where N_{apnea} and $N_{hypopnea}$ are the number of apnea and hypopnea occurrences during sleep. T_{sleep} is the duration of sleep time.

The AHI-based criteria for diagnosing and grading OSAHS severity in PSG monitoring are shown in Table 2. It is clear that the diagnostic criteria for children vary significantly from those applicable to adults, owing to the disparities in physiology, metabolism, and sleep rhythms between these age groups. Current guidelines [11] suggest that the AHI thresholds for detecting OSAHS severity in children should be set at 1, 5 and 10 to define mild, moderate and severe OSAHS. The data from SCMC contains PSG reports of pediatric patients. The annotation files with AHI information from CHAT database are available, all of which can be used as criteria for controlled experiments conducted in this study.

2.2. Preprocessing

The normal SpO_2 value of the oximetry used in this study ranges from 35% to 100%. In the preprocessing phase, common blood oxygen abnormalities were systematically classified into three main categories.

(1) The SpO_2 values fall within the normal range but the data fluctuation does not align consistently with physiological norms. In the CHAT dataset, the SpO_2 change rate is used as the standard of measuring the SpO_2 fluctuation. Taha et al. [26] defined oxygen desaturation as a drop in SpO_2 with a rate of fall greater than 0.1%/s and less than 4%/s, indicating that fluctuations within this range are considered reasonable. Therefore, we define the first type of abnormality as SpO_2 desaturation with a rate of fall exceeding 4%/s. Subsequently, a moving average technique is applied to address outliers. The window size is set to 10 s, which means that detected outliers will be replaced by the average result of the first 10 s. In the SCMC dataset, an additional index, the Perfusion Index (PI), is introduced to identify this type of abnormality. Experimental observations suggest that during this abnormality, the PI of the pulse wave signal is generally very low. Moreover, it was observed that within the SCMC dataset, instances where the PI registered below 4 corresponded to low accuracy in SpO_2 measurements. Consequently, in this dataset, abnormal data segments were identified by vigilant monitoring of the PI values. Due to the lack of PI signals in the CHAT dataset, the SpO_2 change rate was utilized as an alternative measure.

(2) The presence of measurement accuracy errors in oximetry may lead to data oscillations. Pulse oximetry uses indirect measurement to obtain SpO_2. Measurement accuracy error makes the measured SpO_2 fluctuate within a certain error range above or below the true value, causing the oxygen curve to exhibit a jagged shape, which acts as continuously jittering in a certain small range. To enhance the smoothness of the original SpO_2 curve while preserving its overall variation properties, we applied a modified mean-filter, as defined in Eq. (2), to the raw SpO_2 data denoted as $\{x_i | i = 1, 2, \ldots, n\}$.

$$x'_i = \frac{1}{m-4}\left(\sum_{k=i-\lceil \frac{m}{2} \rceil}^{i+\lfloor \frac{m}{2} \rfloor} x_k - x_{max1} - x_{max2} - x_{min1} - x_{min2}\right), \lceil \frac{m}{2} \rceil \le i \le n-m \quad (2)$$

where x_{max1} and x_{max2} represent the maximum value of the raw SpO_2 data and x_{min1} and x_{min2} represent the minimum values of the raw SpO_2 data. The variable m corresponds to the size of the sliding window. Through extensive experimentation, it was observed that if m is too small, the influence of the sudden change of SpO_2 value on the smoothness of the curve cannot be eliminated. Conversely, when m is too large, the resulting curve becomes overly smooth, leading to inaccurate detection of oxygen desaturation events and potential misses in their identification. Optimal results were obtained with m set to 15, achieving a balance where the original trend of SpO_2 changes is well preserved, and simultaneously, the curve is adequately smoothed.

Following the application of Eq. (2) to the SpO_2 data, only the first $\lceil \frac{m}{2} \rceil$ data points and the last $\lfloor \frac{m}{2} \rfloor$ data points remain unprocessed. Thus, we use Eq. (3) to do further processing.

$$x'_i = \begin{cases} \frac{1}{\lfloor \frac{m}{2} \rfloor} \sum_{k=i}^{i+\lceil \frac{m}{2} \rceil - 1} x_k, i = 1, 2, \ldots, \lceil \frac{m}{2} \rceil - 1, \lceil \frac{m}{2} \rceil \\ \frac{1}{\lfloor \frac{m}{2} \rfloor} \sum_{k=i-\lfloor \frac{m}{2} \rfloor + 1}^{i} x_k, i = n - \lfloor \frac{m}{2} \rfloor + 1, \ldots, n-1, n \end{cases} \quad (3)$$

(3) In the SCMC dataset, data from accelerometers is employed to assist SpO_2 preprocessing to eliminate isolated SpO_2 fluctuations induced by obvious body movements. Since the CHAT dataset lacks accelerometer signals in its PSG data, this step is omitted during processing. We denote the motion level as $accLevel_i$, with values of 0, 1, and 2 signifying stable, mild, and strong motion levels, respectively.

If $accLevel_i = 0$ or $accLevel_i = 1$:

$$x''_i = \begin{cases} \frac{1}{5} \sum_{k=0}^{4} x'_{i-k}, i \ge 5 \\ x'_i, i \le 4 \end{cases} \quad (4)$$

When $accLevel_i = 2$, the SpO_2 for the subsequent 30 s requires update. Through statistical analysis. it was observed that the SpO_2 value tends to be erratic within 30 s after a significant increase in the variance of acceleration. If the absolute difference between x_i and x_{i+1} exceeds the threshold $L = 3$, the SpO_2 value will be considered unreliable and processed as follows.

$$x''_i = \begin{cases} \frac{1}{10} \sum_{k=0}^{9} x'_{i-k}, |x'_i - x'_{i+1}| > L \\ x'_i, other \end{cases} \quad (5)$$

2.3. Methods

In this section, we provide a comprehensive exposition of the proposed method. Firstly, a model for identifying oxygen desaturation is introduced. Subsequently, the crucial aspect of pseudo-oxygen desaturation events in the context of apnea and hypopnea detection is addressed. Based on this, an algorithm for the detection of oxygen desaturation events was developed. Then, a preliminary algorithm for detecting apnea and hypopnea events is proposed. Afterward, we explore the detailed implementation of the ERD-GA, utilizing an elite retention strategy and dynamic crossover and mutation for fine-tuning model parameters. Finally, the evaluation metrics used to assess the proposed method, as well as the statistical analysis techniques, were described.

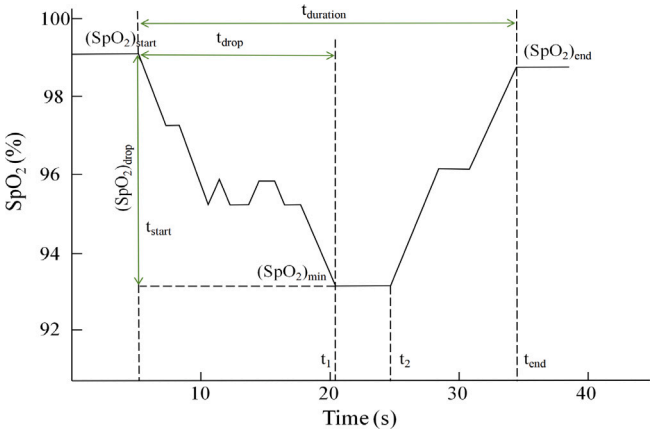

Fig. 1. Oxygen curve of a desaturation event.

Table 3
Oxygen desaturation parameters.

Parameter symbols	Explanation of parameters
t_{start}	Start time of oxygen desaturation
t_{end}	End time of oxygen desaturation
t_1	Start time of the lowest blood oxygen saturation range
t_2	End time of the lowest blood oxygen saturation range
$t_{duration}$	Duration of oxygen desaturation
t_{drop}	Duration of continuous oxygen decrease
$(SpO_2)_{start}$	SpO_2 at the start of oxygen desaturation
$(SpO_2)_{min}$	Lowest SpO_2 during oxygen desaturation
$(SpO_2)_{end}$	SpO_2 at the end of oxygen desaturation
$(SpO_2)_{drop}$	Maximum SpO_2 drop induced by oxygen desaturation

2.3.1. Oxygen desaturation detection model

During apnea or hypopnea episodes in patients with OSAHS, the modulation of respiratory system causes depletion of oxygen within the thoracic cavity and subsequent desaturation in blood oxygen saturation for a specific period. As the apnea reaches a certain threshold, the body typically responds with an awakening mechanism, prompting the reopening of the airway and resumption of normal breathing. This enables sufficient oxygen to be drawn into the chest cavity, leading to the restoration of oxygen saturation levels. Therefore, an oxygen desaturation event curve exhibits a "V" shape, characterized by an initial decrease followed by a subsequent rise. An example of a typical oxygen desaturation event is shown in Fig. 1.

Ten feature parameters are identified to characterize blood oxygen desaturation events. The specifics of these parameters are enumerated in Table 3. Given that the lowest blood oxygen levels may persist for a duration within an oxygen event, we introduce t_1 and t_2 to represent the descending endpoint and ascending starting point respectively. As a standard, a single apnea event usually endures no longer than three minutes. We set a fixed upper limit of 180 s for the duration of oxygen desaturation events.

2.3.2. Pseudo-oxygen desaturation events

When a respiratory event occurs, the resulting oxygen desaturation persists for a specific duration, characterized by a distinct downward trend. However, not all observed oxygen desaturations stem from apnea or hypopnea events. In this paper, pseudo-oxygen desaturation events refer to reductions in oxygen levels caused by non-physiological factors, such as equipment malfunction, external interference, or abnormal

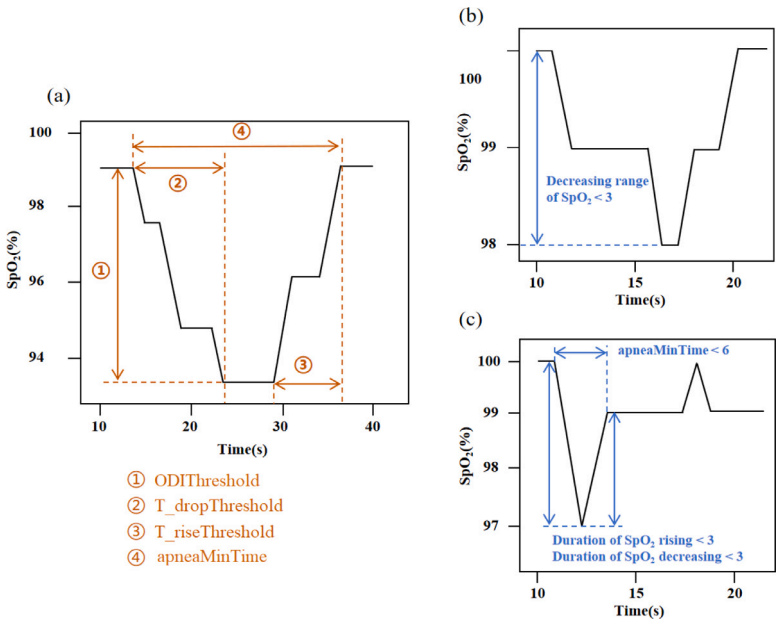

Fig. 2. (a) Example of oxygen desaturation event and (b),(c) Examples of pseudo-oxygen desaturation events.

data processing during oxygen saturation monitoring. Although SpO_2 data may show a decreasing trend, these events do not represent true physiological conditions. Our focus is on optimizing parameters for detecting oxygen desaturation events, and filtering out pseudo-events is a crucial aspect of the process. After analyzing SpO_2 data from various patients, we found that pseudo-oxygen desaturations in the SpO_2 curves often exhibit $t_{duration}$ values that are too short or $(SpO_2)_{drop}$ values that are too low, failing to satisfy the diagnostic criteria for apnea and hypopnea events. Additionally, we observed that the shortest pseudo-desaturation event lasts only 2 s, with a mere 1% drop in oxygen levels.

In this study, pediatric oxygen desaturation events are defined as a drop in oxygen saturation by at least 3% o from the baseline value, lasting for a minimum of 3 s. Additionally, the recovery time from the lowest oxygen saturation level back to baseline must also last at least 3 s, with the total duration of the desaturation event, including recovery, being at least 6 s.

In Fig. 2, the left side illustrates a typical example of a normal oxygen desaturation event, while the right side features two instances of pseudo-oxygen desaturation events. In Fig. 2(b), the decrease in SpO_2 is only 2%, and in Fig. 2(c), the duration of SpO_2 rising/decreasing, as well as the apneaMinTime(Minimum duration of oxygen desaturation), do not meet the necessary judgment criteria. Fig. 2(a) emphasizes the importance of the four parameter indicators marked as ①, ②, ③ and ④ in our assessment.

Table 4 provides the ranges for the four parameters, which will be used in the proposed oxygen saturation detection algorithm. These defined ranges serve as criteria for distinguishing and filtering out pseudo-oxygen desaturation events, ensuring the identification of actual respiratory events. The sequence numbers in explanations of parameters corresponds with sequence numbers in Fig. 2(a). The rationale behind setting these detection parameters is explained below.

(1) A hypopnea event involves an oxygen desaturation of 3% or more, while apnea events typically result in a more significant decrease. To align with diagnosis standards and accommodate population specificity, the threshold for oxygen desaturation events (ODIThreshold) is set within the range of [3, 4].

(2) Based on our analysis of PSG reports, pediatric oxygen desaturation events are observed to last for more than two respiratory cycles. Considering that one respiratory cycle for a child lasts approximately 3 to 5 s during the day, with an extension during sleep, we set the maximum limit for the event duration at 15 s.

(3) For a V-shaped oxygen desaturation event, we set the thresholds for the duration of the initial SpO_2 drop and the subsequent rise within the range of 3 to 10 s to ensure unbiased evaluation metrics.

Table 4
Parameters for oxygen desaturation events detection.

Parameter symbols	Explanations of parameters	Range
①ODIThreshold	Decreasing range of SpO_2	[3,4]
②T_dropThreshold	Duration of SpO_2 decreasing	[3,10]
③T_riseThreshold	Duration of SpO_2 rising	[3,10]
④apneaMinTime	Duration of oxygen desaturation	[6,15]

Table 5
Parameters for apnea and hypopnea events detection.

Parameter symbols	Explanation of parameters	Range
SpO_2_dropThreshold	SpO_2 variation during oxygen desaturation	[5,8]
SpO_2_riseThreshold	SpO_2 variation during oxygen saturation in recovery	[3,8]
riseDropRate	Ratio of SpO_2 rising to decreasing duration	[0.5,1)

2.3.3. Preliminary algorithm for apnea–hypopnea detection

Following the exclusion of pseudo oxygen desaturation events, the remaining desaturation events can be categorized into apnea and hypopnea events. The parameters for identifying apnea and hypopnea events in this paper are listed in Table 5. Based on PSG data collected from SCMC, it has been observed that approximately 90% of oxygen desaturation levels during apnea and hypopnea events fall within the range of 5% to 8%. This range is further utilized to set the value for SpO_2_dropThreshold. And the parameter SpO_2_riseThreshold for characterizing SpO_2 recovery is set within the range of 3% to 8%. In addition, the duration of SpO_2 rising during apnea events is typically shorter than the decreasing duration, and in some cases, the ratio between the two can be as low as 0.5 during a brief oxygen desaturation event. Therefore, the lower limit of the riseDropRateis set to 0.5.

Empirically, if a respiratory event meets the criteria: (1) SpO_2_dropThreshold ≥ 5 (2)SpO_2_riseThreshold ≥ 4 (3) riseDropRate ≥ 0.8, it will be classified as an apnea event. Otherwise, it will be classified as a hypopnea event. With the provided parameters above, both apnea and hypopnea events can be tentatively identified. However, as the

inherent complexity and variability of oxygen desaturation events in real-world scenarios, it is crucial to accurately identify the characteristic points of these events. This is essential for distinguishing them from pseudo-oxygen desaturation events, ensuring the accurate calculation of subsequent AHI indicators.

2.3.4. Optimizing apnea–hypopnea detection: the ERD-GA model

(1) Optimization with genetic algorithm

In order to improve the accuracy of the OSAHS diagnosis, it is important to optimize critical parameters within the apnea–hypopnea detection model.

As a heuristic optimization algorithm, genetic algorithm(GA) is used to solve complex searching and optimization problems by simulating the mechanisms of genetic and natural selection during biological evolution [27]. In practice, GAs represent individuals using chromosomes, which are composed of genes. Each chromosome encodes a possible solution, typically as a coded string. Each segment of this string, or gene, corresponds to a specific parameter value of the problem. Genetic operations such as crossover and mutation alter the combination of genes between different chromosomes, producing new solutions. A fitness function evaluates how well each individual in the population performs; the higher the fitness, the better the solution that individual represents. Individuals with higher fitness have a greater chance of being retained or reproduced in the next generation. The search space consists of all possible solutions, with its size and dimensions determined by the number and range of parameters. Through iterative evolution across generations, individuals with higher fitness are selected, and crossover and mutation operations modify gene combinations to optimize the search space.

We initially applied the standard GA to optimize the parameters of both the oxygen desaturation event detection model and the apnea–hypopnea event detection model. The search space for the desaturation model comprises the threshold values of the four parameters in Table 4, while the search space for the apnea–hypopnea model comprises the threshold values of the three parameters in Table 5. These optimizations aimed to improve event detection accuracy, followed by relevant data analysis. However, the optimization results were not satisfactory, possibly due to early convergence or stagnation issues within the standard GA. If the crossover and mutation probabilities are set too low or too high, they can impact the retention of high-fitness individuals, preventing the model from reaching optimal parameter values. Consequently, this may affect the final accuracy of AHI calculations in both datasets.

To address these issues, this paper proposes novel strategies in population updating, individual selection, crossover and mutation to improve the performance of the standard GA, resulting in an algorithm termed ERD-GA.

(2) Implementation of ERD-GA

a. Elite retention strategy

If the population update is solely derived from the offspring, a significant amount of information from the preceding generation will be discarded. This is particularly noticeable when the fitness of the offspring experiences a sharp decline, often caused by a high probability of crossover and mutation among the exceptional individuals from the parent generation.

In such a scenario, individuals with high fitness from the parent generation may be lost. The elite retention strategy is proposed to preserve the two best solutions generated in the current iteration, retain the two current optimal solutions generated in this iteration but not to participate in migration and mutation operations. These two solutions are subsequently updated before the next iteration, thereby allowing the newly generated solutions in each iteration to build upon the foundation of the original optimal solutions. Fig. 3 illustrates the schematic flowchart of the improved population update.

In Fig. 3, the population is denoted as cT, the auxiliary population as cP and the new population as cN. The size of cT is set to N = 50 and

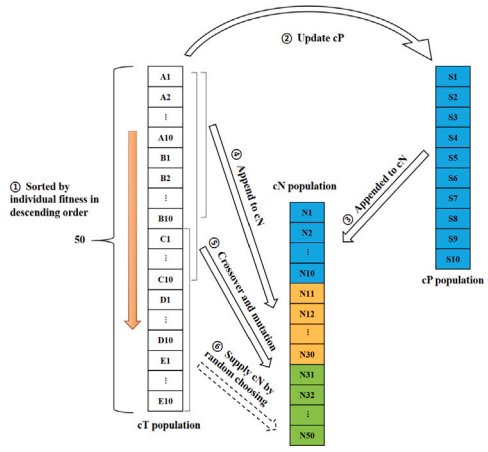

Fig. 3. Flowchart of the ERD-GA.

the size of cP' is 20%×N. The population cP consistently retains the most well-adapted individuals throughout the process. It is created and updated at each generation by completely being created with the 10 best of the current generation. Whenever cT is updated for individual selection, it is first sorted in descending order based on individual fitness. Subsequently, individuals from cP are incorporated into the new population cN. The initial 20 individuals from cT are then replicated into cN, while the last 20 individuals in cN are generated through random pairwise crossover or mutation of the first 30 individuals. This process enriches the variety of individuals. If a chromosomal genetic expression falls outside the parameter range, the latter 30 individuals from cT are randomly chosen for supplementation. Finally, cN is utilized as the next generation of cT for the iterative search of merits.

b. Dynamic crossover and mutation

Dynamic crossover and mutation probabilities are utilized to enhance the algorithm's robustness in both the initial and final stages. The two probabilities decrease gradually as the number of iterations progresses, as shown in Eq. (6).

$$\begin{cases} P_c = P_{c0}\, e^{-(N/N_{\max})} \\ P_m = P_{m0}\, e^{-(N/N_{\max})} \end{cases} \tag{6}$$

where P_c and P_m denote the crossover probability and the mutation probability, respectively, with initial values P_{c0} and P_{m0}. N_{max} stands for the maximum number of iterations, while N represents the current iteration count. In our work, P_{c0} is set to 0.85 and P_{m0} is set to 0.03. In the initial stages, when the population's fitness is widely dispersed, it is advisable to set P_c and P_m to relatively large values. This aids in the removal of suboptimal individuals and the introduction of new, potentially superior ones, thereby enhancing global search capabilities. As the population's fitness becomes more concentrated in the later stages, it is beneficial to decrease P_c and P_m o safeguard the fittest individuals and facilitate convergence. Additionally, prioritizing the best crossover population allows for the exploration of potential opportunities to generate even more highly-adapted individuals based on the foundation of high-quality individuals.

c. Design of fitness functions

In the design of the ERD-GA model for pediatric OSAHS detection, a crucial aspect is the development of fitness curves for oxygen desaturation detection and apnea–hypopnea detection, respectively. The fitness function directly impacts the algorithm's performance and efficiently reflects the gap between each individual and the one with the optimal solution.

In this study, the algorithms for detecting oxygen desaturation and apnea–hypopnea events are presented separately.

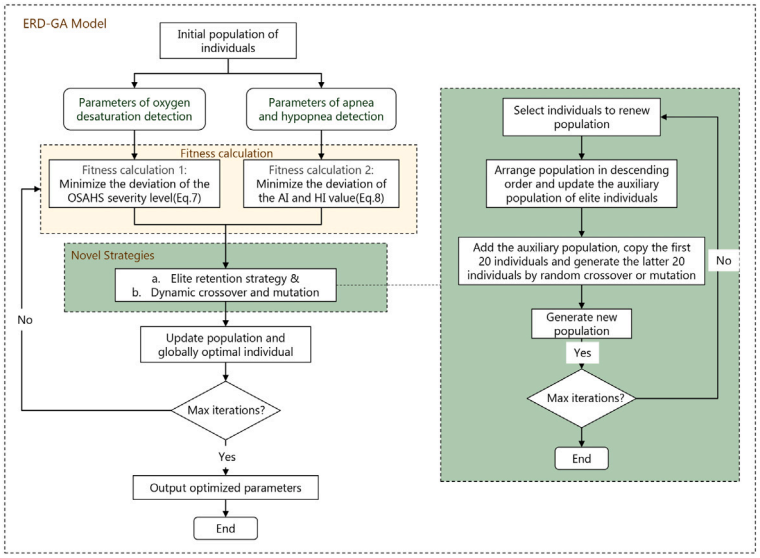

Fig. 4. Flowchart of the enhanced apnea–hypopnea detection using ERD-GA.

The oxygen desaturation detection algorithm uses the parameters defined in Table 4, and its fitness function is defined in Eq. (7).

$$\begin{cases} fitness = \frac{1}{d} \\ d = \sum_{i=1}^{k} |degree\_PSG_i - degree\_cal_i| \end{cases} \tag{7}$$

where Degree_PSG_i and Degree_cal_i denote the severity of OSAHS assessed by the PSG report and model for the ith data, respectively. In this work, 150 iterations of population evolution were conducted with an initial population of 30 during the process.

The optimization of oxygen desaturation screening strategy focuses on minimizing the deviation between model evaluation and PSG reporting results. This is achieved by associating OSAHS severity levels (none, mild, moderate, severe) with numerical values (0, 1, 2, 3). This indirect regulation addresses differences in AHI and ODI indices.

The algorithm for detecting apnea–hypopnea uses the parameters defined in Table 5 and its fitness function is defined in Eq. (8).

$$\begin{cases} fitness = \frac{1}{difAI} \\ difAI = \sum_{i=1}^{k} |AI\_PSG_i - AI\_cal_i| \end{cases} \tag{8}$$

where AI_PSG_i and AI_cal_i present the AI obtained from the PSG report and model of the i_{th} data, respectively. In this work, 100 iterations of population evolution were conducted with an initial population size of 20 during the ERD-GA process.

(3) Key steps in ERD-GA

The overall concept for the ERD-GA is outlined as follows:

Step 1: Optimal coding method and population initialization are crucial for algorithm success. Genes are constructed based on the number and range of parameters for optimization. In this paper, binary codification is adopted.

Step 2: Define a suitable fitness function and evaluate the fitness of individuals within the generated population.

Step 3: Implement the elite retention strategy, along with dynamic crossover and mutation, as elaborated in the previous section. This increases the likelihood of generating high-fitness individuals and preserves them for the subsequent generation.

Step 4: Check if the termination criteria are satisfied; if not, iterate through the aforementioned steps.

Based on these steps, the flowchart of the proposed apnea–hypopnea detection model is illustrated in Fig. 4.

2.3.5. Statistical analysis

In this study, we conducted a thorough evaluation of the ERD-GA method, employing various statistical tests to ensure a comprehensive assessment. The Bland–Altman analysis takes center stage, providing insights into the agreement between ERD-GA results and PSG outcomes across subjects. Notably, we extend this analysis by incorporating results from traditional GA, offering a comparative perspective and emphasizing the advancements our method brings. The SCMC dataset was used for parameter optimization in both the oxygen desaturation detection algorithm and the apnea–hypopnea detection algorithm, with the optimized algorithms subsequently evaluated on the independent CHAT dataset.

Recognizing that Bland–Altman analysis has its limitations, it is complemented with the intra-class correlation coefficient (ICC), a widely accepted metric in conservative medicine for evaluating test-retest reliability [28]. ICC provides a detailed understanding of the correlation and consistency between measurements, strengthening the reliability assessment.

To further validate the accuracy of OSAHS diagnosis achieved by ERD-GA, a confusion matrix is introduced. This matrix serves as a robust tool to evaluate the cyclic detection performance of our proposed method, providing detailed insights into correct and incorrect identifications across all OSAHS severity levels.

By combining these diverse statistical approaches, we aim to present a thorough and robust evaluation of the ERD-GA method, revealing its effectiveness in pediatric OSAHS detection.

3. Results

3.1. Optimized parameters

In our study, the standard GA was initially used to optimize the model parameters. As shown in Fig. 5, AHI values are significantly overestimated compared to those reported by PSG, except in cases of severe OSAHS. This suggests that the standard GA-based model tends to overestimate the severity of OSAHS, particularly in cases of mild and moderate severity.

To improve the standard genetic algorithm, we proposed the ERD-GA algorithm. Fig. 6 illustrates the fitness curves for oxygen desaturation and apnea–hypopnea detection, optimized by ERD-GA.It is evident from Fig. 6(a) that the proposed strategy for optimizing parameters in oxygen desaturation detection attains its highest adaptation with an OSAHS severity bias of only 1, indicating a deviation in diagnosis for

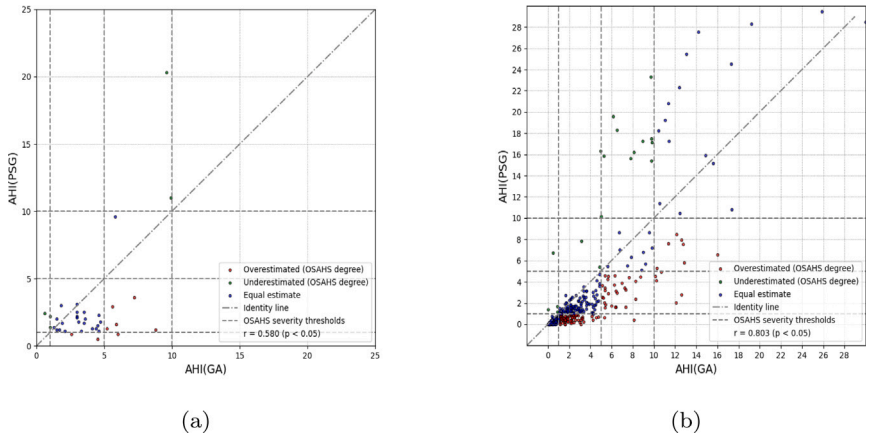

Fig. 5. Comparison of AHI estimates by standard GA on (a) SCMC dataset and (b) CHAT dataset.

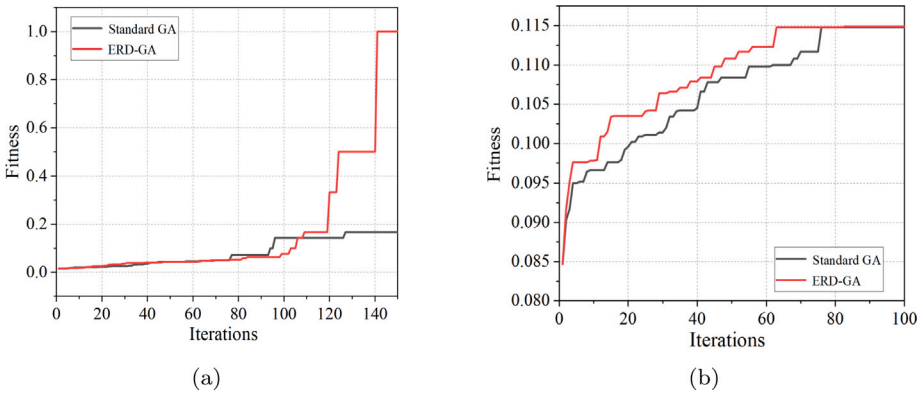

Fig. 6. Comparison of fitness curves between ERD-GA and standard GA in SCMC dataset (a) Oxygen desaturation detection (b) Apnea–hypopnea detection.

Table 6
Results of optimized parameters.

ICC	95% confidence interval		Optimized parameters	Result	Type of detection
	Lower bound	Upper bound			
0.951	0.921	0.978	ODIThreshold apneaMinTime T_dropThreshold T_riseThreshold	3 9 6 7	Oxygen desaturation detection
0.985	0.973	0.993	riseDropRate dropThreshold riseThreshold	0.84 6 6	Apnea–Hypopnea detection

only one individual. Fig. 6(b) shows that both ERD-GA and the standard GA yielded similar fitness values, the ERD-GA exhibited superior global search efficiency, achieving faster convergence and attaining the global optimal solution.

The results of this optimization process are detailed in Table 6. Noteworthy are the ICC values of 0.951 and 0.985 for the two types of detection, indicating a high level of agreement with the PSG results.

3.2. Calculation of AHI

In Fig. 7, scatter plots illustrate the AHI values calculated by the ERD-GA for both datasets in comparison to the AHI values reported in PSG. The 'r' values denote Pearson's correlation coefficient. Dashed lines represent the conventional OSAHS severity classes, while the dash-dotted line signifies the identity line. Notably, the ERD-GA exhibits a tighter clustering of data points around the diagonal line in contrast to the standard GA in Fig. 5(a) and Fig. 5(b). This is evidenced by the Pearson's correlation coefficient values of 0.969 and 0.927, respectively. The graphical representation of the results indicates that the ERD-GA provides more accurate AHI estimates.

The results in Table 7 demonstrate that the ERD-GA outperforms the standard GA in both datasets. For SCMC subjects, the mean absolute AHI estimation errors are 0 event/h for those without OSAHS, and 0.26, 0.40, and 5.40 events/h for those with mild, moderate, and severe conditions, respectively. In the CHAT dataset, the mean absolute AHI (ERD-GA) estimation errors are 0.35, 0.84, 2.85, and 5.15 events/h for subjects without OSAHS, and those with mild, moderate, and severe conditions, respectively. Given the substantial volume of data in the CHAT dataset, Bland–Altman plots of the AHI estimates generated by the ERD-GA are provided in Fig. 7(c) and (d), where the bias of agreement is presented in events/h.

3.3. Evaluation of OSAHS severity diagnosis performance

The entire dataset from SCMC and 318 data from the CHAT dataset are used to create a confusion matrix. Fig. 8 shows the confusion

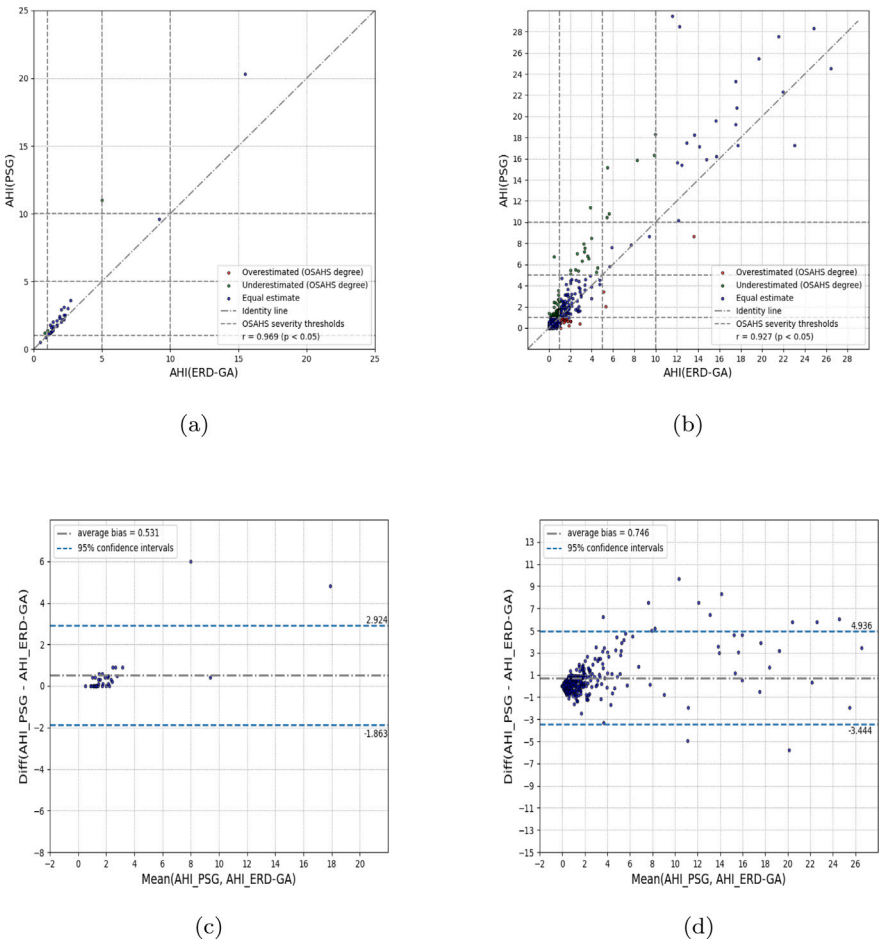

Fig. 7. Comparison of AHI estimates by ERD-GA on (a) SCMC dataset and (b) CHAT dataset, along with Bland–Altman plots of AHI estimates in (c) SCMC dataset and (d) CHAT dataset.

Table 7
Comparison of mean absolute AHI estimation errors.

OSAHS	GA(SCMC)	ERD-GA(SCMC)	GA(CHAT)	ERD-GA(CHAT)
None	3.6	0	1.06	0.35
Mild	1.9	0.26	1.71	0.84
Moderate	3.8	0.40	3.59	2.85
Severe	5.90	5.40	7.27	5.15

matrix of ERD-GA model on both the SCMC and CHAT datasets, which illustrates the model's capability to categorize the severity of OSAHS. Specifically, the ERD-GA accurately classified subjects without OSAHS and those with moderate OSAHS in the SCMC dataset, aligning with the actual OSAHS severity groups. Notably, the accuracy of diagnosis significantly improved for patients with mild and severe OSAHS. Fig. 8(d) shows the ERD-GA correctly assigned 87.31% (117/134), 68.38% (93/136), 84.21% (16/19), and 86.21% (25/28) of subjects to their respective OSAHS severity groups.

The algorithms were further evaluated in a binary classification context, distinguishing between no-OSAHS and OSAHS, using decision thresholds of 1, 5, and 10 events/h. The results, summarized in Table 8, highlight the enhanced classification performance of the proposed ERD-GA model compared to the standard GA model across all threshold values. Notably, the highest accuracy for both algorithms is achieved at a decision threshold of 10 events/h, which represents a more conservative criterion for pediatric OSAHS. Specifically, the ERD-GA model achieves a correct decision rate of 97.22% and 98.12% in the SCMC and CHAT datasets, respectively, while the GA model achieves 94.44% and 92.45%, respectively.

Table 8
Performance comparison in binary classification.

	GA(SCMC)			ERD-GA(SCMC)		
AHI (events/h)	1	5	10	1	5	10
Sens (%)	0	81.82	100	100	100	100
Spec (%)	96.97	100	0	96.97	100	50
Acc (%)	88.89	83.33	94.44	97.22	100	97.22
	GA(CHAT)			ERD-GA(CHAT)		
AHI (events/h)	1	5	10	1	5	10
Sens (%)	85.87	68.75	39.29	97.83	91.67	84.51
Spec (%)	80.60	87.41	95.86	86.57	99.268	99.66
Acc (%)	72.64	88.05	92.45	81.45	97.42	97.92

Sens: sensitivity; Spec: specificity; Acc: accuracy.

4. Discussion

In this study, we investigated the effectiveness of the proposed algorithm in improving the diagnostic capabilities for pediatric apnea–hypopnea events. The enhanced genetic algorithm, ERD-GA, integrates an elitism retention strategy along with dynamic crossover and mutation probabilities to optimally select various parameters for screening oxygen desaturation events. Controlled experiments were conducted on two distinct pediatric patients datasets to demonstrate the diagnostic performance of the model, with one dataset sourced from the CHAT to enhance overall reliability. The obtained results demonstrate a notably high sensitivity and accuracy in classifying AHI levels.

Existing models for OSAHS detection have primarily relied on algorithms extracting time–frequency domain features from blood oxygen

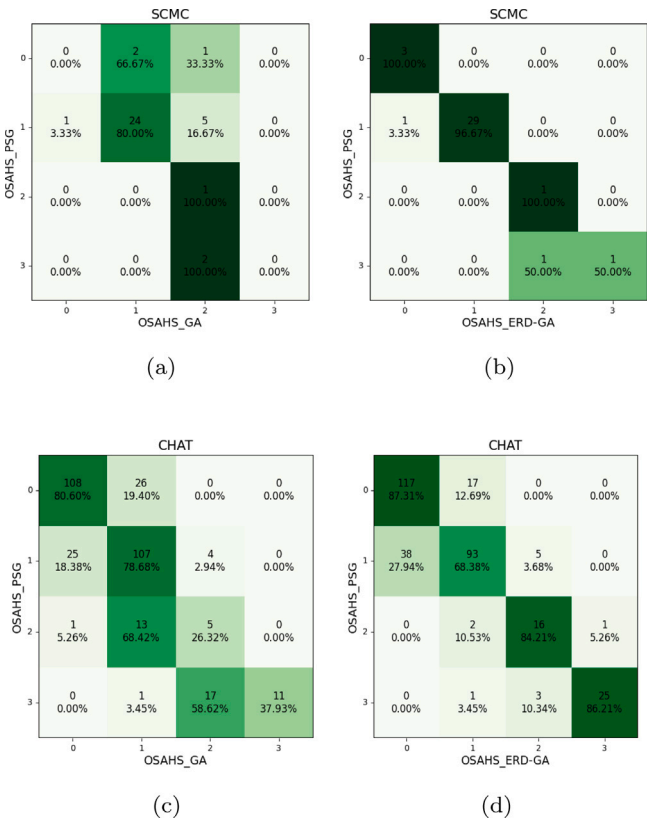

Fig. 8. Confusion matrix of the ERD-GA's AHI for canonical AHI thresholds in the SCMC and CHAT datasets.

signals employing deep learning techniques. Recently, several deep learning based approaches have emerged. Notably, Biswal et al. [29] and Nikkonen et al. [30] achieved impressive accuracies in classifying subjects into the four severity degrees of adult OSAHS. In contrast, our study focused on the characteristic changes in blood oxygen signals during oxygen desaturation events, specifically in pediatric patients. This distinction is crucial, as the grading of AHI in pediatric patients differs from that in adults, with a greater emphasis on precise AHI classification.

4.1. Enhanced genetic algorithm (ERD-GA)

In previous studies, such as Tang et al. [23], the application of traditional GA for optimizing OSAHS detection models encountered challenges due to algorithmic randomness, especially with small datasets, leading to local optimal solutions. To address this, we introduced an ERD-GA with an elitism retention algorithm, coupled with dynamic crossover and mutation. This modification resulted in an increased retention rate of individuals with the highest fitness, leading to improved global optimal solutions.

Fig. 4 illustrates the specific steps of the ERD-GA algorithm, emphasizing the safeguarding of top-performing individuals in each population update selection. This enhancement significantly contributed to the algorithm's ability to find global optimal solutions more efficiently. The ERD-GA demonstrated the ability to achieve the highest fitness value in fewer iterations.

4.2. Diagnostic performance

Our proposed model demonstrated significant performance enhancements compared to the traditional GA, evident in both CHAT and SCMC datasets. Rather than focusing solely on clinical Heart Rate Variability (HRV) features and deep learning methods, our approach concentrated on characterizing the changes in SpO_2 signals during apnea–hypopnea events and refining model parameters. By optimizing these parameters, we achieved a highly effective automatic approach for calculating the AHI index, reducing the overestimation of apnea–hypopnea events and enhancing diagnostic performance.

4.3. Comparison with other studies

Recent studies have explored various approaches, including extracting time–frequency domain features, applying machine learning, and employing multi-signal fusion, to enhance diagnostic capabilities for OSAHS. We conducted a comparative analysis with existing methods on the CHAT dataset. Martín-Montero et al. [31] introduced three new spectral bands of ECG, demonstrating significant associations with SAHS disease severity and achieving 82.8% accuracy and 0.796 AUC for a 10 events/h threshold. Vaquerizo-Villaret al. [32] employed a CNN architecture, utilizing Bayesian optimization to estimate the number of apnea events. The AHI CNN exhibited a higher four-class Cohen's kappa in CHAT compared to ODI3 (0.515 vs. 0.417) and AHI MLP (0.515 vs. 0.377). Jiménez-García et al. [33] input AF and SpO_2 signals into a 2D CNN architecture, achieving AHI cutoffs of 84.64%, 93.46% and 94.44% for 1, 5, and 10 events/h in CHAT.

Table 9 summarizes the performance of our study against state-of-the-art studies aimed at detecting pediatric OSAHS on the CHAT dataset. Notably, none of the studies reported a higher sensitivity for AHI severity compared to the proposed ERD-GA in the CHAT dataset. Our study consistently demonstrated higher diagnostic sensitivity, particularly in cases with lower AHI thresholds, compared to other studies presented. This highlights the robustness and efficacy of our model in evaluating OSAHS screening, a critical aspect of medical prevention.

The reported diagnostic accuracies in these recent studies vary, ranging from 52.60%–84.64% for the AHI threshold of 1 event/h, 76.40%–97.40% for the threshold of 5 events/h, and 82.80%–97.80% for AHI threshold of 10 events/h. Our study demonstrates superior accuracy compared to these previous works. Particularly noteworthy is our model's exceptional diagnostic sensitivity for the 1 event/h threshold, outperforming all other models. Moreover, at critical AHI thresholds of 5 events/h and 10 events/h, our model achieves sensitivities of 91.67% and 84.51%, respectively.

4.4. Limitations

Although our work has made significant progress, there are certain aspects that require further consideration. First, due to the corruption of some original files, not all data from the CHAT dataset could be used, introducing limitations to our study. Additionally, the absence of an annotation file for the lowest oxygen saturation in the CHAT dataset restricts the applicability of our method for patients with hypoxemia.

Furthermore, our classification is tailored specifically for obstructive sleep apnea events, without accounting for central sleep apnea. This discrepancy arises from the fact that central respiratory events entail a cessation of respiratory effort, as conventionally inferred from the abdominal and thoracic respiratory effort belts of the PSG [35]. To achieve a precise diagnosis of central sleep apnea, a broader range of physiological signals should be taken into account. Future studies should encompass a diverse array of signals and investigate the differences and correlations in oxygen desaturation events between obstructive and central sleep apnea.

It is worth noting that the parameters L and mean window length, used in preprocessing, are based on empirical data. Additionally, the parameter thresholds in Tables 4 and 5 are derived solely from empirical settings within the SCMC database, which may not be applicable to other populations or conditions. The lack of validation on larger or more diverse datasets limits the generalizability of the results. Future studies could validate these parameters using larger sample sizes and broader databases, or explore alternative parameter settings that may be more suitable.

Table 9
Performance evaluation of state-of-the-art studies for pediatric OSAHS Detection using the CHAT dataset.

Studies	Dataset	AHI (events/h)	Methods	Sens (%)	Spec (%)	Acc (%)
Martín-Montero et al. [31]	CHAT	1	New HRV spectral bands of interest	42.50	72.30	52.60
		5		50.00	80.90	76.40
		10		63.80	84.70	82.80
CalderLón et al. [34]	CHAT	5	Extracted features from SpO_2 signal used in the CHAT/ML-based classifier	62.00	96.00	79.00
Jiménez-García et al. [33]	CHAT	1	Airflow and SpO_2 signals/ a 2D convolutional neural network	82.43	92.54	84.64
		5		80.22	99.07	93.46
		10		71.43	98.11	94.44
Vaquerizo-Villaret al. [32]	CHAT	1	CNN architecture	71.20	81.80	77.60
		5		83.70	100.00	97.40
		10		83.90	99.30	97.80
Ours	CHAT	1	ERD-GA	97.83	86.57	81.45
		5		91.67	99.26	97.42
		10		84.51	99.66	98.12

5. Conclusions

In this study, we introduced a novel approach referred to as ERD-GA by implementing a refined elitism retention strategy and dynamic crossover and mutation probabilities within the standard GA framework, aimed at optimizing parameters in the OSAHS detection model. This enhancement has led to a notable improvement in the diagnostic capacity of the pediatric OSAHS detection model.

Given that many pediatric apnea-hypopnea events are closely associated with oxygen desaturation and that sleep apnea syndrome often results in intermittent nocturnal hypoxemia, our approach primarily focuses on detecting OSAHS in children by analyzing the characteristic changes in SpO_2 signals during apnea–hypopnea events. We conducted a comparative analysis by utilizing SpO_2 recordings obtained concurrently with PSG monitoring to assess the indicators of AHI calculated by our proposed model. Subsequently, we evaluated the performance of the ERD-GA in characterizing different degrees of OSAHS in children. The findings of our study demonstrate a notable improvement in the diagnostic capacity for pediatric OSAHS provided by our model.

CRediT authorship contribution statement

Linwen Jiang: Writing – original draft, Visualization, Software, Methodology, Formal analysis, Data curation. **Min Li:** Writing – review & editing, Supervision, Conceptualization. **Jing Jiang:** Data curation, Formal analysis, Visualization, Writing – review & editing. **Qinghua Hu:** Writing – review & editing, Formal analysis.

Declaration of competing interest

The authors declare that they have no known competing financial interests or personal relationships that could have appeared to influence the work reported in this paper.

Data availability

Data will be made available on request.

References

[1] Ajay S. Nathan, Richard D. Hubbell, Jessica R. Levi, Management of children with co-occurring sleep disordered breathing and hearing loss, Int. J. Pediatr. Otorhinolaryngol. 163 (2022) 111367.
[2] Gili Kadmon, et al., Validation of a pediatric obstructive sleep apnea screening tool, Int. J. Pediatr. Otorhinolaryngol. 77 (9) (2013) 1461–1464.
[3] Mandip Kang, et al., Trends in diagnosing obstructive sleep apnea in pediatrics, Children 9 (3) (2022) 306.
[4] Khin Hnin, et al., The impact of ethnicity on the prevalence and severity of obstructive sleep apnea, Sleep Med. Rev. 41 (2018) 78–86.
[5] Christopher M Cielo, et al., Neck fat and obstructive sleep apnea in obese adolescents, Sleep 44 (11) (2021) zsab158.
[6] Elizabeth M Cespedes Feliciano, et al., Objective sleep characteristics and cardiometabolic health in young adolescents, Pediatrics 142 (1) (2018).
[7] Leon S Siriwardhana, et al., Children with down syndrome and sleep disordered breathing display impairments in ventilatory control, Sleep Med. 77 (2021) 161–169.
[8] F Blanc, et al., Respiratory polygraphy in children: Feasibility in everyday practice in an ENT department and value of automatic detection of respiratory events, Eur. Ann. Otorhinolaryngol. Head Neck Dis. 136 (4) (2019) 235–240.
[9] Madeline JL Ravesloot, et al., Perioperative care of patients with obstructive sleep apnea undergoing upper airway surgery: a review and consensus recommendations, JAMA Otolaryngol.–Head Neck Surg. 145 (8) (2019) 751–760.
[10] Richard B Berry, et al., The AASM manual for the scoring of sleep and associated events, in: Rules, Terminology and Technical Specifications, Darien, Illinois, American Academy of Sleep Medicine, vol. 176, 2012, p. 2012.
[11] Working group of Chinese guideline for the diagnosis, et al., Chinese guideline for the diagnosis and treatment of childhood obstructive sleep apnea (2020), Pediatr. Invest. 5 (03) (2021) 167–187.
[12] Robert T Brouillette, et al., Nocturnal pulse oximetry as an abbreviated testing modality for pediatric obstructive sleep apnea, Pediatrics 105 (2) (2000) 405–412.
[13] Catherine Jonas, et al., Comparison of nocturnal pulse oximetry with polysomnography in children with sleep disordered breathing, Sleep Breath. 24 (2020) 703–707.
[14] Andy Cheuk-ting Hou, et al., Use of pulse oximetry to screen for infant obstructive sleep apnoea, Pediatr. Respirol. Crit. Care Med. 5 (4) (2021) 70–76.
[15] Olaf Oldenburg, et al., Improving nocturnal hypoxemic burden with transvenous phrenic nerve stimulation for the treatment of central sleep apnea, J. Cardiovasc. Transl. Res. 14 (2021) 377–385.
[16] Daniel Álvarez, et al., Automated screening of children with obstructive sleep apnea using nocturnal oximetry: an alternative to respiratory polygraphy in unattended settings, J. Clin. Sleep Med. 13 (5) (2017) 693–702.
[17] Xenia LR Hoppenbrouwer, et al., Night to night variability of pulse oximetry features in children at home and at the hospital, Physiol. Meas. 42 (10) (2021) 104003.
[18] Fernando Vaquerizo-Villar, et al., Utility of bispectrum in the screening of pediatric sleep apnea-hypopnea syndrome using oximetry recordings, Comput. Methods Prog. Biomed. 156 (2018) 141–149.
[19] Gastón Schlotthauer, et al., Screening of obstructive sleep apnea with empirical mode decomposition of pulse oximetry, Med. Eng. Phys. 36 (8) (2014) 1074–1080.
[20] Alfredo Burgos, et al., Real-time detection of apneas on a PDA, IEEE Trans. Inf. Technol. Biomed. 14 (4) (2009) 995–1002.
[21] Fernando Vaquerizo-Villar, et al., Detrended fluctuation analysis of the oximetry signal to assist in paediatric sleep apnoea–hypopnoea syndrome diagnosis, Physiol. Meas. 39 (11) (2018) 114006.
[22] Maria Pia Villa, et al., Diagnosis of pediatric obstructive sleep apnea syndrome in settings with limited resources, JAMA Otolaryngol.–Head Neck Surg. 141 (11) (2015) 990–996.
[23] Youyuan Tang, et al., An OSAHS detection method based on genetic algorithm for parameter optimization, in: Proceedings of the Eighth Asia International Symposium on Mechatronics, 2022, pp. 2148–2158.
[24] Carole L Marcus, et al., A randomized trial of adenotonsillectomy for childhood sleep apnea, N. Engl. J. Med. 368 (25) (2013) 2366–2376.
[25] Richard B Berry, et al., Rules for scoring respiratory events in sleep: update of the 2007 aasm manual for the scoring of sleep and associated events: deliberations of the sleep apnea definitions task force of the American academy of sleep medicine, J. Clin. Sleep Med. 8 (5) (2012) 597–619.

[26] BH Taha, et al., Automated detection and classification of sleep-disordered breathing from conventional polysomnography data, Sleep 20 (11) (1997) 991–1001.
[27] S Katoch, S.S. Chauhan, V. Kumar, A review on genetic algorithm: past, present, and future, Multimed. Tools Appl. 80 (2021) 8091–8126.
[28] P. Siva Krishna, P.V. Gopi Krishna Rao, Fractional-order PID controller for blood pressure regulation using genetic algorithm, Biomed. Signal Process. Control 88 (2024).
[29] Siddharth Biswal, et al., Expert-level sleep scoring with deep neural networks, J. Am. Med. Inform. Assoc. 25 (12) (2018) 1643–1650.
[30] Sami Nikkonen, et al., Artificial neural network analysis of the oxygen saturation signal enables accurate diagnostics of sleep apnea, Sci. Rep. 9 (1) (2019) 13200.
[31] Adrián Martín-Montero, et al., Heart rate variability spectrum characteristics in children with sleep apnea, Pediatr. Res. 89 (7) (2021) 1771–1779.
[32] Fernando Vaquerizo-Villar, et al., A convolutional neural network architecture to enhance oximetry ability to diagnose pediatric obstructive sleep apnea, IEEE J. Biomed. Health Inform. 25 (8) (2021) 2906–2916.
[33] Jorge Jiménez-García, et al., A 2D convolutional neural network to detect sleep apnea in children using airflow and oximetry, Compute. Biol. Med. 147 (2022) 105784.
[34] José Miguel Calderón, et al., Development of a minimally invasive screening tool to identify obese pediatric population at risk of obstructive sleep apnea/hypopnea syndrome, Bioengineering 7 (4) (2020) 131.
[35] Frederik Massie, et al., Central sleep apnea detection by means of finger photoplethysmography, IEEE J. Transl. Eng. Health Med. 11 (2023) 126–136.